



Angle Inclination Effect on Vortex Breakdown Zone in Rotating Flow Inside a Vertical Conical Container

Bouhant Hassene^{*}, Bessaih Rachid¹

LEAP Laboratory, Department of Mechanical Engineering, Faculty of Technology Sciences, Constantine 1- Frères Mentouri University, Constantine 25000, Algeria

Corresponding Author Email: hassene.bouhant@umc.edu.dz

Copyright: ©2024 The authors. This article is published by IIETA and is licensed under the CC BY 4.0 license (<http://creativecommons.org/licenses/by/4.0/>).

<https://doi.org/10.18280/ijht.420117>

ABSTRACT

Received: 6 November 2023

Revised: 24 January 2024

Accepted: 29 January 2024

Available online: 29 February 2024

Keywords:

rotating flow, conical container, vortex breakdown, Reynolds number, aspect ratio

This study presents a numerical investigation of the swirling flow inside a vertical conical container. The container is filled with liquid metal (Prandtl number, $Pr=0.015$), with the upper disc rotating at a fixed angular velocity while the bottom disc remains stationary. The sidewall of the container is rigid and inclined. In such a configuration, a phenomenon called vortex breakdown can occur, acting like a stagnation point against the axial flow pattern; the purpose of this study is to illustrate how the inclination of the cylinder's sidewall can affect the vortex breakdown and their emergence and suppression. The study encompasses a range of Reynolds numbers ($1000 \leq Re \leq 2500$) and various aspect ratios ($1 \leq H/R \leq 2.4$) where three different angles of inclination ($\alpha=5^\circ, 10^\circ, \text{ and } 15^\circ$) are considered. The results are obtained by resolving numerically the governing equations using the finite volume technique. Our findings indicate that, for a given Reynolds number ($Re=2000$) and aspect ratios in the range of $1.2 \leq H/R \leq 1.6$, the inclination of the sidewall leads to an earlier occurrence of vortex breakdown. On the other hand, for aspect ratios in the range of $1.8 \leq H/R \leq 2.2$, the inclination of the sidewall results in the suppression of vortex breakdown. Furthermore, we have observed that the critical Reynolds number (Re_c) at which vortex at which vortex breakdown occurs for aspect ratios of $A=H/R=1.4, 1.8, \text{ and } 2.2$ increases with the increasing angle of inclination α .

1. INTRODUCTION

Numerous studies have focused on rotating flows in the last several years, driven by their industrial significance and application across various engineering domains. These flow patterns are encountered in various engineering applications, including viscometers, turbo machinery, and crystal production using the Czochralski growth method [1-4]. The first publication dedicated to such flow patterns appeared in 1921 and was presented by Von Karman [5], one of the eminent figures in fluid mechanics. He examined the problem of fluid flow induced by the rotation of an infinite disk, where the fluid far from the disk remains stationary. By applying the principle of similarity, he could transform the system of Navier-Stokes equations into a pair of nonlinear equations in axial coordinates. If we denote the fluid's rotation speed far from the disk as Ω_f and the disk's rotation speed as Ω_d , Von Karman investigated the case ($\Omega_f=0, \Omega_d \neq 0$). Subsequently, Bodewadt [6] delved into the complementary problem, examining the flow of a viscous and incompressible fluid in uniform rotation on a stationary disk ($\Omega_f \neq 0, \Omega_d=0$).

In his experiments, Vogel [7, 8] investigated the fluid flow in a vertical cylinder generated by the rotation of a bottom disk. He determined a curve illustrating the boundaries within which the vortex known as "breakdown" would appear, representing the stability limits in the ($H/R, Re=\Omega R^2/\nu$) plane,

where H is the cylinder's height, R is the radius, and Re is the rotational Reynolds number using the same geometric configuration as considered in Vogel's work, with $H/R=1.59$ and $\Omega R^2/\nu=1.58$.

Using the laser-induced fluorescence visualization method, Escudier [9] observed the steady swirling flow of a fluid (glycerin/water) in a cylindrical chamber with a rotating bottom. The author highlighted the emergence of one, two, and three vortex breakdown bubbles. A stability map was developed by varying two parameters: the aspect ratio of the cylinder (H/R) and the rotational Reynolds number ($\Omega R^2/\nu$).

In another study, Escudier et al. [10] presented numerical results for the flow within a truncated cone generated by the rotation of an end wall. Vortices were suppressed beyond a certain wall inclination angle for converging geometries (where the radius increases as one approaches the rotating end wall) and diverging geometries. Simultaneously, Moffat vortices of growing strength and extent appeared in the corner between the lateral and non-rotating end walls. In the case of diverging geometry, a recirculation zone emerged on the lateral wall and merged with the Moffat vortices. Streamline patterns facilitated the identification of coherent flow phenomena consistent with the calculated pressure variation around the domain's periphery.

Bessaih and colleagues [11-13] conducted a series of numerical studies in 1999, 2003, and 2009, investigating the

stability of rotating liquid metal flows in cylindrical enclosures under magnetohydrodynamic (MHD) influence. Bessaih et al. [11] conducted a numerical study on the laminar MHD (Magneto Hydro Dynamic) flow of liquid metal within a cylindrical enclosure with an aspect ratio equal to 1. The upper wall of the enclosure is rotating, and the system is subjected to a vertical external magnetic field. The authors achieved a good agreement between asymptotic and numerical results, demonstrating that primary flow can be controlled by a careful selection of the electrical conductivity of the walls of the enclosure. Furthermore, Bessaih et al. [12] conducted a numerical and analytical study of the stable laminar flow generated by a rotating disk at the top of a cylinder with an aspect ratio H/R equal to unity. The cylinder is filled with liquid metal and subjected to an axial magnetic field. The authors solved the governing equations of the flow using a finite volume method. They provided various analytical velocity formulas and demonstrated that, in the presence of a magnetic field, the analytical velocity profiles near the end disks, obtained for a high value of the magnetic interaction parameter N , exhibit an excellent agreement with those obtained from numerical simulations. Thus, they highlighted the significance of the electrical conductivity of the container walls (both disks and the side wall) in controlling the flow. Their research also explored how magnetic fields and wall conductivity affected flow patterns and heat transfer, especially for high Prandtl number flows [13]. Without a magnetic field, heat transfer behaved like a cylindrical tank with a propeller. In the presence of a magnetic field, significant heat transfer reduction occurred. Using magnetic fields to suppress convection during crystal growth is a well-established technique, with ongoing discussions involving experiments and numerical simulations.

de Moro Martins et al. [14] conducted a numerical simulation investigating vortex breakdown in constrained rotating flows. They examined two enclosed geometries, cylindrical and conical-cylindrical, with flow rotation initiated by a continuously rotating bottom wall. The study initially validated their computational code by comparing numerical results with experimental data. Subsequent simulations explored the transitional regime and vortex breakdown formation by varying parameters like the Reynolds number and aspect ratio. The investigation encompassed steady and transient scenarios, considering turbulence and non-turbulence models. Interestingly, distinctions emerged in the vortex breakdown process within conical-cylindrical geometries compared to cylindrical geometries.

Mahfoud et al. [15] carried out a numerical investigation into the flow resulting from the counter-rotation of the upper and lower disks inside a truncated conical enclosure filled with liquid metal under the influence of an axial magnetic field. The upper and lower disks rotated in opposite directions at constant angular velocities Ω . Their research uncovered that the external magnetic field effectively restrained fluid motion, prompting a shift to axisymmetric flow. Furthermore, they noted that the critical thresholds (Re_{cr}) corresponding to $m=1$ modes increased with higher Hartmann numbers (Ha). Lastly, they constructed a diagram illustrating the stability (Re - Ha) based on the numerical insights from this study.

In this research, we conduct a 3-D numerical analysis of the rotating flow within a vertical conical cavity. The container contains a liquid metal with a low Prandtl number ($Pr=0.015$). The upper disc is subjected to a fixed angular velocity, while the lower disc remains stationary. The container's sidewall is

rigid and inclined. The study encompasses a range of Reynolds numbers ($1000 \leq Re \leq 2500$) and various aspect ratios ($1 \leq H/R \leq 2.4$).

Moreover, we examine three distinct angles of inclination ($\alpha=5^\circ, 10^\circ, \text{ and } 15^\circ$). The primary objective of our study is to explore how these variables influence the emergence and suppression of vortex breakdown. Additionally, we aim to identify the critical Reynolds number (Re_{cr}) at which vortex breakdown occurs for different aspect ratios ($A=H/R$) and various inclination angles (α).

2. GEOMETRIC CONFIGURATION AND MATHEMATICAL MODELING

The study focuses on a vertical conical cavity with a base radius R , top radius R_t and height H , defined by its aspect ratio ($A=H/R$), as presented in Figure 1. A low Prandtl number liquid metal ($Pr=0.015$) is present within this cavity. In this setup, the upper-endwall rotates at a constant angular velocity Ω , while the lower disk remains stationary. The lateral wall is both rigid and inclined. The fluid's physical properties are considered constant, except density, which exhibits a linear variation with temperature according to the Boussinesq approximation.

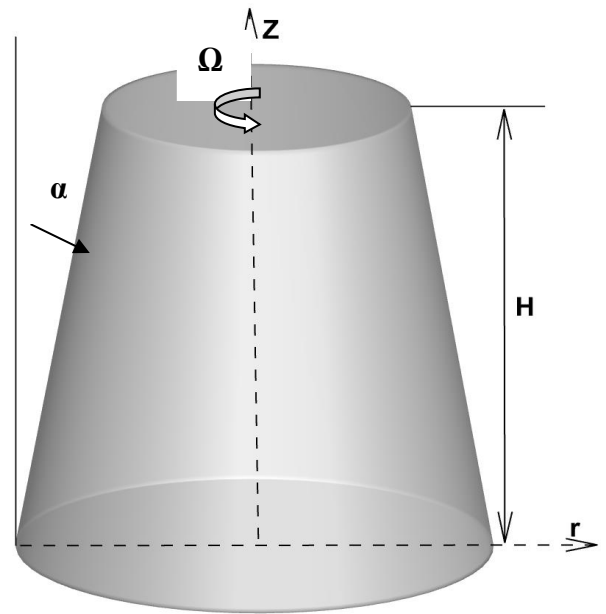


Figure 1. Geometric configuration and boundary conditions

2.1 Governing equations

As previously described, we assume that the flow exhibits laminar, incompressible, steady, and three-dimensional characteristics to determine the flow pattern within the conical container with a rotating end wall. Furthermore, by introducing dimensionless parameters for time, length, velocity, and pressure, represented as $1/\Omega$, ΩR , and $\rho(\Omega R)^2$, respectively, we can formulate the governing equations in a dimensionless manner as follows:

$$\nabla U = 0 \quad (1)$$

$$\frac{\partial U}{\partial \tau} + U \cdot \nabla U = -\nabla P + \frac{1}{Re} \nabla^2 U \quad (2)$$

where,

∇ : is the Laplacian operator,

U : the velocity vector (U, V, W),

τ : the dimensionless time,

P : the dimensionless pressure,

and Re is the Reynolds number based on the radius of the rotating end-wall calculated as follows:

$$Re = \frac{\Omega R_t^2}{\nu}$$

where, ν kinematic viscosity, Ω : angular velocity, R_t : rayon of the upper disc

The provided Eqs. (1) to (2) are resolved while considering the following set of initial and boundary conditions.

At $\tau = 0$:

$$u=0, v=0, w=0, (0 < r < R, 0 < z < H),$$

For $\tau > 0$:

At $z=H$ and $0 < r < R$:

$$u=0, v=0, w=r,$$

At $z=0$ and $0 < r < R$:

$$u=0, v=0, w=0,$$

At $r=R$ and $0 < z < H$:

$$u=0, v=0, w=0.$$

3. NUMERICAL METHOD

The equations described in references 1-2 are resolved by applying the finite volume method outlined by Bodewadt [6]. Specifically, the vector components (u, v , and w) are discretely stored at staggered locations, while the scalar variable (P) is situated at the central points of these discrete volumes. To handle the convection term, a second-order central difference scheme is employed, as suggested in reference 20. The SIMPLER algorithm, detailed in the study of Bodewadt [6], also manages the coupling between pressure and velocity. The convergence criteria is declared met for a given time step when the maximum difference between consecutive iterations becomes less than $10e-6$ at that particular time step.

4. GRID INDEPENDENCE STUDY AND VALIDATION

The choice of mesh and its impact on the numerical solution are crucial aspects of numerical simulation. Therefore, it is essential to select the most suitable mesh type for the specific problem and assess its effect on the results by conducting calculations with different mesh configurations.

For this study, the hexahedral mesh type was chosen for the considered geometry due to its superiority, particularly in its impact on the flow structure compared to the tetrahedral type. The impact study was also performed using four different grids. The results are presented in Figure 2, which shows that the axial velocity profiles along the centreline become nearly superimposed when transitioning from the $80 \times 80 \times 160$ mesh grid to the $90 \times 90 \times 180$ mesh grid. Based on the findings of this study, the preferred mesh choice for solving the given problem is the $80 \times 80 \times 160$ node grid in the radial, circumferential, and axial directions, respectively.

To ensure the validity of our current numerical model, we have undertaken a rigorous process of validation by comparing our numerical simulations with previously published results in

the scientific literature; the validation involves a direct comparison with the results obtained by Escudier et al. [10] the authors analyzed the flow within a truncated cone created by the rotation of one of the end walls. In Figure 3, we have presented the recreated streamlines for a convergent geometry at $Re=1854$, with an inclination angle of the container sidewall set at $\alpha=7$ degrees.

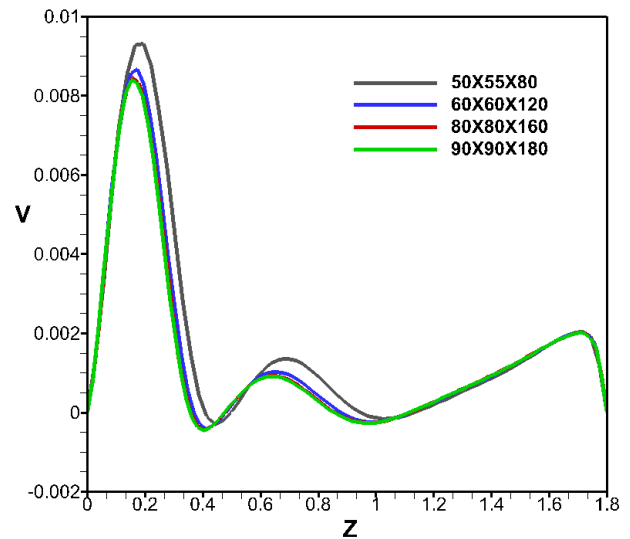


Figure 2. Axial velocity distribution along the centerline of the cylinder for different mesh grids with $A=H/R=1.8$, $Re=2000$, $\alpha=10^\circ$

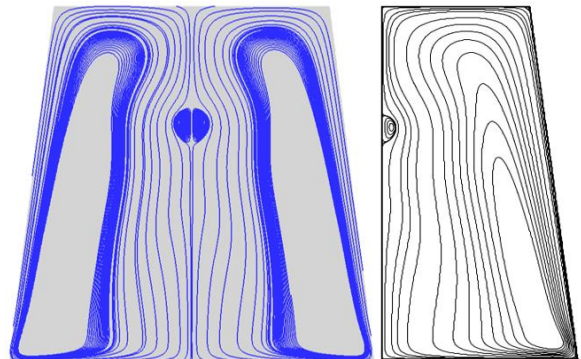


Figure 3. Comparison with the numerical results presented by Escudier in 2007 [10]: Streamlines contours in a cylinder with an aspect ratio $H/R=2$, angle of inclination $\alpha=7^\circ$ at (a) $Re=1854$

5. RESULTS

The findings from numerical simulations are showcased for the stable flow generated by the rotation of the upper disk within a conical vertical cylinder containing a viscous fluid. Several aspect ratios ranging from 1 to 2.4, along with three different inclination angles ($\alpha=5^\circ, 10^\circ$, and 15°), have been taken into account. It has been observed that, for aspect ratios $1.2 \leq H/R \leq 1.6$, the inclination of the wall leads to the earlier onset of vortex breakdown, whereas for aspect ratios $1.8 \leq H/R \leq 2.2$, the inclination of the wall leads to the suppression of vortex breakdown. It is important to emphasize that the fundamental flow characteristics were initially examined by Von Kármán [5]. In his analysis, the bottom disk, which rotates, functions as a pump by drawing fluid axially

and expelling it outward in a spiral mode; within a confined cylinder, this fluid follows a spiral path along the cylindrical wall as it enters through the stationary top wall, subsequently changing its direction to the axial flow as within the Reynolds number range associated with it approaches the rotating bottom wall. This spiral motion initially leads to increased swirl velocity due to the conservation of angular momentum, ultimately forming a concentrated vortex. Additionally, the results are presented the appearance of the recirculation bubble. The calculations were conducted for various inclination angles to investigate their influence on the position and disappearance of vortex breakdown.

5.1 Inclination effect of sidewall

To demonstrate the influence of the conical shape of the cylinder (the inclination of the cylinder's sidewall) on the flow streamlines and the occurrence or suppression of vortex breakdown, we present in Figure 4 the evolution of streamlines plotted in meridian planes (XZ) for a fixed value of Reynolds number (Re) of 2000 and three different conical.

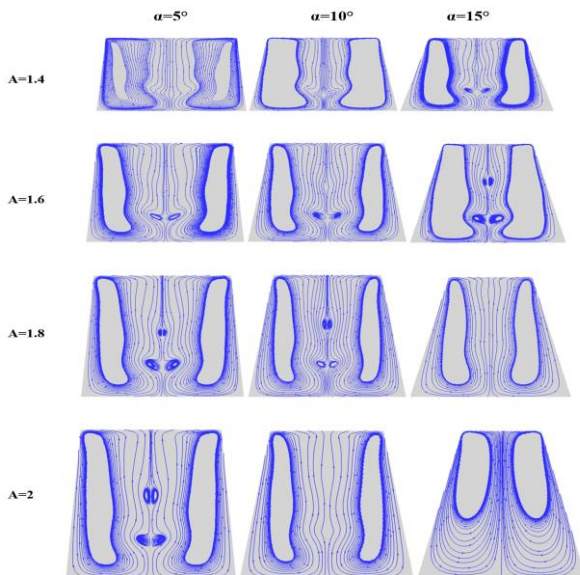


Figure 4. The evolution of streamlines in meridian planes (XZ) at Re=2000 for three different conical shapes with $\alpha=5^\circ$, 10° , and 15° , and various aspect ratios $A=H/R$: 1.4, 1.6, 1.8, and 2.0, respectively

Shapes characterized by the inclination angle $\alpha=5^\circ$, 10° , and 15° , along with aspect ratios $A=H/R$: 1.4, 1.6, 1.8, and 2.0, respectively. It is observed that for the case of an aspect ratio $A=1.4$ when the inclination angle increases from $\alpha=10^\circ$ to 15° , the vortex breakdown appears, as illustrated in the second row of Figure 4. In the case of an aspect ratio $A=1.6$, an increase in the inclination angle from $\alpha=10^\circ$ to 15° reveals a second set of vortex breakdowns, as shown in the second row of Figure 4. Conversely, for both cases with aspect ratios $A=1.8$ and $A=2$, increasing the inclination angle leads to the disappearance of vortex breakdown, as illustrated in the third and fourth rows of Figure 4, respectively. It is also noticeable that, for inclination angles $\alpha=5^\circ$ and $\alpha=10^\circ$, increasing the aspect ratio leads to the emergence of vortex breakdown. However, at an inclination angle of $\alpha=15^\circ$, increasing the aspect ratio to $A=1.6$ results in the appearance of a second set of vortex breakdowns. However, the vortex breakdown disappears when the aspect ratio reaches $A=1.8$ and beyond. In summary, for aspect ratios $A<1.6$, an

increase in the inclination of the sidewall leads to vortex breakdown. In contrast, for aspect ratios $A>1.6$, an increase in the inclination of the sidewall leads to the suppression of vortex break down. This can be explained by considering that, for aspect ratios $A<1.6$, the propagation or dissipation of kinetic energy within the fluid induced by the rotating disc becomes more significant as the inclination of the sidewall increases. Conversely, for aspect ratios $A>1.6$, the dissipation of kinetic energy within the fluid supplied by the rotating disc becomes less significant as the inclination of the sidewall increases.

5.2 Ratio aspect effect

To further illustrate the influence of aspect ratios $A=H/R$ on the behaviors of the appearance, position, or disappearance of vortex breakdown in a convergent conical geometry ($\alpha=10^\circ$), we can take, for example, $Re=2000$ with a convergent conical shape characterized by $\alpha=10^\circ$. By increasing the aspect ratios $A=H/R$ from 1.2 to 2.2, as presented in Figure 5, showing the evolution of streamlines in meridian planes (XZ), The flow exhibits vortex breakdown for aspect ratios within the range of $1.6 \leq A=H/R \leq 2$. however, when $H/R<1.6$ and $H/R>2$, no vortex breakdown was observed, as evidenced by the streamlines presented in the figure. This pattern closely aligns qualitatively with the findings reported by Mahfoud et al. [16].

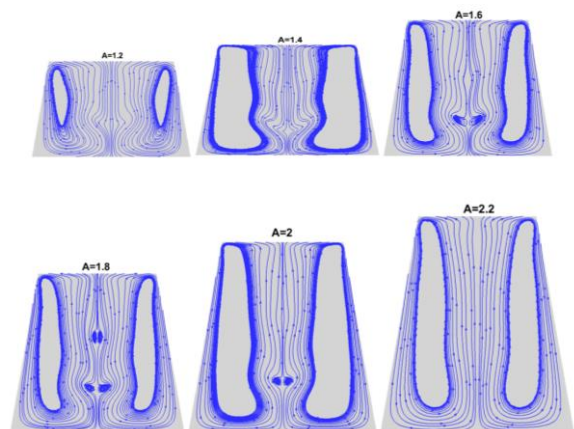


Figure 5. The evolution of streamlines in meridian planes (XZ) at Re=2000 and $\alpha=10^\circ$ for various aspect ratios $A=H/R$: 1.4, 1.6, 1.8, 2.0, and 2.2

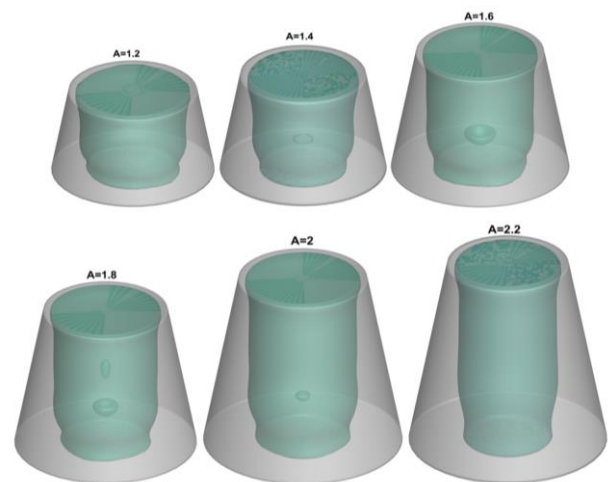


Figure 6. Spatial evolution of zero axial velocity for various aspect ratios at Re=2000

Figure 6 presents the spatial configuration of zero axial velocity values at varying aspect ratios under $Re=2000$ and $\alpha=10^\circ$. In this scenario, vortex breakdown becomes apparent; the recirculation bubble behaves like an obstacle against the axial flow when $1.6 \leq A=H/R \leq 2$. Flow is redirected around the bubble, giving rise to a downstream wake region characterized by significantly reduced velocities. Within the vortex breakdown bubble, the impact of viscosity and inertia is negligible, resulting in zero axial velocity. It is worth noting that no such bubble is observed for $A=H/R$ values below 1.6 or above 2.

5.3 Reynolds Re effect

5.3.1 Case $A=H/R=1.4$

For this low aspect ratio $A=1.4$, simulations were conducted for three different inclination angles, namely $\alpha=5^\circ$, $\alpha=10^\circ$, and $\alpha=15^\circ$, with a gradual increase in Reynolds numbers ranging from 1000 to 2000. The objective was to analyze the hydrodynamic evolution of the flow and determine the thresholds at which bifurcations in the flow structure occur. Figure 7 displays streamlines plotted in the cylinder's meridian plane (XZ).

For each scenario, as the Reynolds number (Re) increases, the deformation of streamlines becomes more pronounced, accompanied by the observation of secondary circulation within each half of the meridian planes. This phenomenon signifies fluid circulation induced by the Ekman pumping effect and the emergence of a pair of vortex breakdowns, where the axial flow is redirected around the recirculation region. This redirection is evident through the divergence of streamlines surrounding the bubble. With a further increase in Re , there is a transformation where the recirculation bubble collapses, forming a spiral column vortex along the axis. This transformation is illustrated in Figure 7 for two specific cases: $Re=2000$ and $\alpha=5^\circ$, as well as $Re=2000$ and $\alpha=10^\circ$.

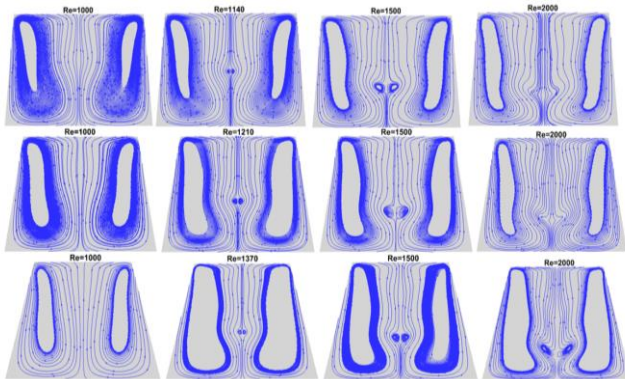


Figure 7. The evolution of streamlines in meridian planes (XZ) at aspect ratios $A=H/R=1.4$ for three different conical shapes with $\alpha=5^\circ$, 10° , and 15° , and various values of Re

The graph presented in Figure 8 illustrates the critical Reynolds values, denoted as Rec , at which vortex breakdown occurs for each inclination angle α , specifically $\alpha=5^\circ$, $\alpha=10^\circ$, and $\alpha=15^\circ$. According to the diagram of Figure 8, Rec increases with an increase in the inclination angle α . The critical Reynolds values, denoted as Rec , marking the onset of vortex breakdown are 1140, 1210, and 1370 for $\alpha=5^\circ$, $\alpha=10^\circ$, and $\alpha=15^\circ$, respectively. These critical thresholds were established by incrementally raising the Reynolds number.

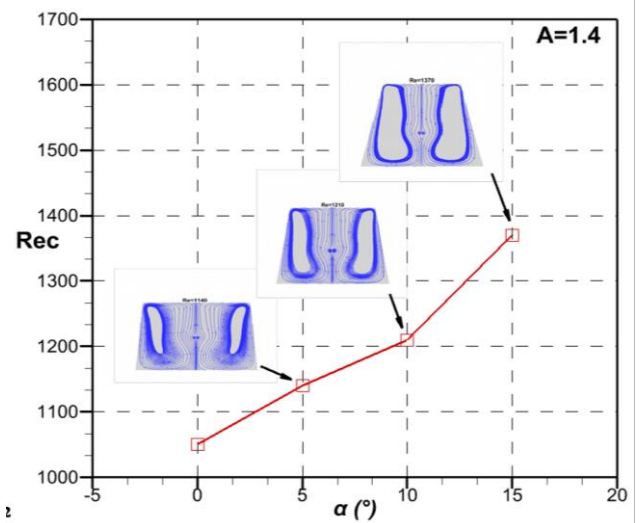


Figure 8. Critical Reynolds Re_c thresholds at which vortex breakdown occurs for $A=H/R=1.4$ and various value of angle of inclination $\alpha=0^\circ$, $\alpha=5^\circ$, $\alpha=10^\circ$

5.3.2 Case $A=H/R=1.8$

For this medium aspect ratio $A=1.8$, simulations were conducted for three different inclination angles, namely $\alpha=5^\circ$, $\alpha=10^\circ$, and $\alpha=15^\circ$, with a gradual increase in Reynolds numbers ranging from 1000 to 2500. However, for the case of $\alpha=15^\circ$, calculations were stopped at $Re=2300$ because the flow became unstable beyond this value, and convergence could not be achieved.

Figure 9 illustrates the path lines of surface streamlines in a meridian plane XZ for $A=1.8$. In the cases of $\alpha=5^\circ$ and $\alpha=10^\circ$, an increase in the Reynolds number initially leads to the appearance of a first pair of vortex breakdown, and with further increases in Reynolds number Re , a second pair of vortex breakdown emerges, as depicted in Figure 9 for $\alpha=5^\circ$ and $Re=2000$, and $\alpha=10^\circ$ and $Re=2000$.

The second recirculation bubble takes shape further downstream of the initial one, featuring a greater axial span yet a reduced diameter compared to the first bubble in the scenario where α equals 5 degrees, and the Reynolds number (Re) is elevated to 2500, these recirculation bubbles dissipate. Conversely, when α is 10 degrees, the downstream recirculation bubble draws nearer to the upstream counterpart, leading to their fusion into a unified recirculation bubble comprised of two separate segments, as illustrated in Figure 9 for $Re=2500$ and $\alpha=10^\circ$.

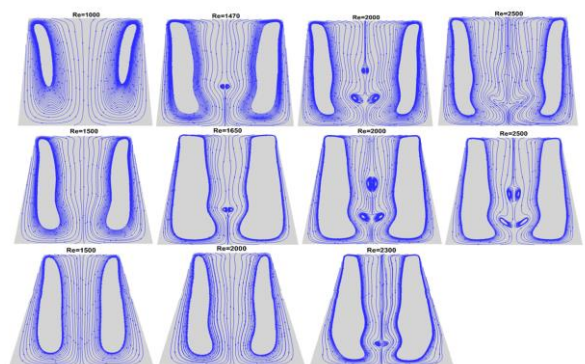


Figure 9. The evolution of streamlines in meridian planes (XZ) at aspect ratios $A=H/R=1.8$ for three different conical shapes with $\alpha=5^\circ$, 10° , and 15° , and various values of Re

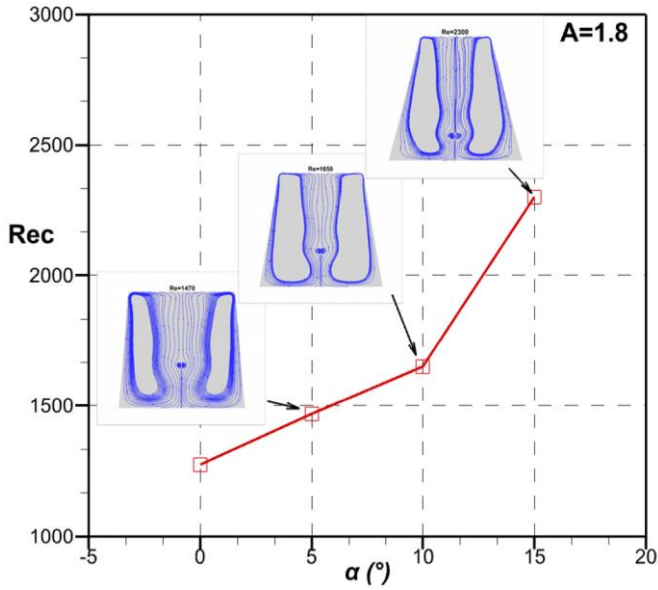


Figure 10. Critical Reynolds Re_c thresholds at which vortex breakdown occurs for $A=H/R=1.8$ and various value of angle of inclination $\alpha=0^\circ$, $\alpha=5^\circ$, $\alpha=10^\circ$

In the case of $\alpha=15^\circ$, it's noteworthy that a single pair of vortex breakdown appears at a significant Reynolds value of 2300.

Figure 10 presents the stability diagram in a $Rec-\alpha$ plane, highlighting the thresholds at which vortex breakdown occurs. It is observed that Rec increases progressively with the inclination angle α . The critical Reynolds values Rec for the appearance of vortex breakdown are 1470, 1650, and 2300 for $\alpha=5^\circ$, $\alpha=10^\circ$, and $\alpha=15^\circ$, respectively.

5.3.3 Case $A=H/R=1.4$

For this higher aspect ratio $A=2.2$, simulations were conducted at three distinct inclination angles: $\alpha=5^\circ$, $\alpha=10^\circ$, and $\alpha=15^\circ$. The Reynolds numbers were gradually increased from 1000 to 2500. However, in the case of $\alpha=15^\circ$, the calculations were halted at $Re=2200$ due to the onset of flow instability, making convergence unattainable.

Figure 11 depicts the trajectories of surface streamlines in the meridian XZ plane for $A=2.2$. In the case of $\alpha=5^\circ$, an initial increase in the Reynolds number results in the appearance of a primary pair of vortex breakdowns.

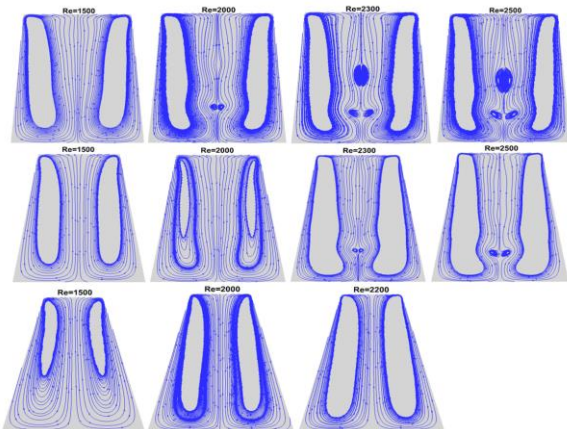


Figure 11. The evolution of streamlines in meridian planes (XZ) at aspect ratios $A=H/R=2.2$ for three different conical shapes with $\alpha=5^\circ$, 10° , and 15° , and various values of Re

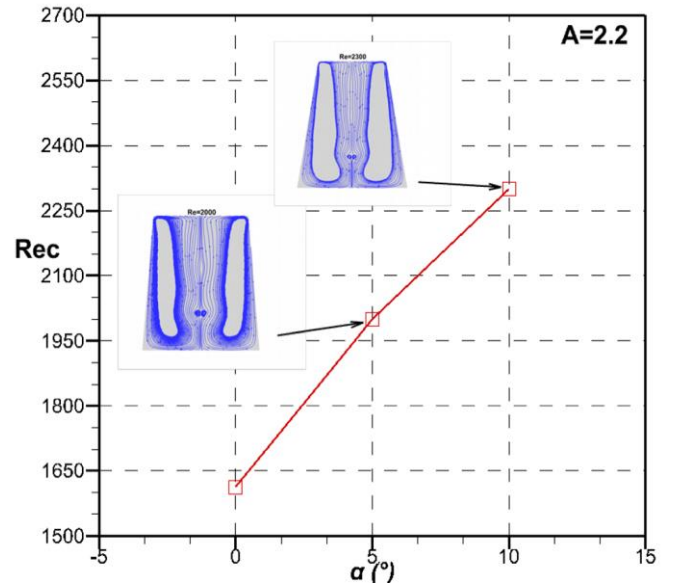


Figure 12. Critical Reynolds Re_c thresholds at which vortex breakdown occurs for $A=H/R=2.2$ and various value of angle of inclination $\alpha=0^\circ$, $\alpha=5^\circ$, $\alpha=10^\circ$

Subsequently, with further increments in the Reynolds number Re , a secondary pair of vortex breakdowns emerges, as illustrated in Figure 11 for $\alpha=5^\circ$ and $Re=2000$, as well as $\alpha=5^\circ$ and $Re=2300$. The second recirculation bubble develops downstream of the first, exhibiting a longer axial extent and a larger diameter than the initial recirculation bubble. Notably, even with the increase in Reynolds number to $Re=2500$, the flow structure had no significant alteration.

In the case of $\alpha=10^\circ$, an increase in Re -up to 2500 results in the appearance of a single recirculation bubble. Conversely, no vortex breakdown is observed for the case of $\alpha=15^\circ$.

Figure 12 presents a stability diagram in the $Rec-\alpha$ plane, highlighting the critical thresholds at which vortex breakdown occurs. It is also observed that Rec increases progressively with the inclination angle α . The critical Reynolds values Rec for the appearance of vortex breakdown are 2000 and 2300 for $\alpha=5^\circ$ and $\alpha=10^\circ$, respectively.

6. CONCLUSIONS

Three-dimensional numerical studies were conducted on the flow inside a vertical conical container. The container is filled with liquid metal (Prandtl number, $Pr=0.015$), with the upper disc rotating at a fixed angular velocity while the bottom disc remains stationary. The sidewall of the container is rigid and inclined. The finite volume method was employed to solve the equations of continuity and momentums. The key findings are as follows:

For a fixed Reynolds number ($Re=2000$), our study reveals that an inclined sidewall influences the occurrence of vortex breakdown. Specifically, within the aspect ratio range of $1.2 \leq H/R \leq 1.6$, an inclined sidewall leads to an earlier onset of vortex breakdown. This effect is noteworthy, demonstrating the system's sensitivity to changes in sidewall inclination.

Conversely, when considering aspect ratios within the range of $1.8 \leq H/R \leq 2.2$, our findings indicate that tilting the sidewall suppresses vortex breakdown. This observation underscores the nuanced interplay between geometric parameters and flow dynamics, emphasizing the potential for sidewall inclination

to act as a control mechanism for vortex breakdown.

Notably, our study shows that the critical Reynolds number (Re_c) at which vortex breakdown occurs for aspect ratios of $A=H/R=1.4, 1.8,$ and 2.2 increases with the angle of inclination (α). This suggests that the inclination angle plays a crucial role in determining the critical conditions for vortex breakdown, highlighting the need for a comprehensive understanding of the system's response to various geometric configurations.

REFERENCES

[1] Wang, L., Horiuchi, T., Sekimoto, A., Okano, Y., Ujihara, T., Dost, S. (2018). Numerical investigation of the effect of static magnetic field on the TSSG growth of SiC. *Journal of Crystal Growth*, 498: 140-147. <https://doi.org/10.1016/j.jcrysgro.2018.06.017>

[2] Ma, N., Walker, J.S., Witkowski, L.M. (2004). Combined effects of rotating magnetic field and rotating system on the thermocapillary instability in the floating zone crystal growth process, *Transactions of the ASME, Journal of Heat Transfer*, 126: 230-235. <https://doi.org/10.1115/1.1666883>

[3] Kharicha, A., Alemany, A., Bornas, D. (2005). Hydrodynamic study of a rotating MHD flow a cylindrical cavity by ultrasound Doppler shift method. *International Journal of Engineering Science*, 43(7): 589-615. <https://doi.org/10.1016/j.ijengsci.2004.09.010>

[4] Spohn, A. (1991). *Écoulement et éclatement tourbillonnaires engendrés par un disque tournant dans une enceinte cylindrique*. Thèse de Doctorat, Université de Grenoble I.

[5] Von Karman, T. (1921). Über laminare und turbulente reibung. *Journal of Applied Mathematics and Mechanics*, 1(4): 233-252. <https://doi.org/10.1002/zamm.19210010401>

[6] Bodewadt, U.T. (1940). Die drehstromung uber festem grund. *Journal of Applied Mathematics and Mechanics*, 20(5): 241-253. <https://doi.org/10.1002/zamm.19400200502>

[7] Vogel, H.U. (1968). Experimentelle Ergebnisse über die laminare Strömung in einen zylindrischen Gehäuse mit darin rotierender Scheibe. *Max Plank Inst. Berichi*, 6.

[8] Vogel, H.U. (1975). Rückströmungsblasen in Drallströmungen. *Festschrift 50 Jahre Max-Plank-Institut für Strömungsforschung*.

[9] Escudier, M.P. (1984). Observations of the flow produced in a cylindrical container by a rotating endwall. *Experiments in Fluids*, 2(4): 189-196. <https://doi.org/10.1007/BF00571864>

[10] Escudier, M.P., O'Leary, J., Poole, R.J. (2007). Flow produced in a conical container by a rotating endwall. *International Journal of Heat and Fluid Flow*, 28(6): 1418-1428. <https://doi.org/10.1016/j.ijheatfluidflow.2007.04.018>

[11] Bessaih, R., Marty, P., Kadja, M. (1999). Numerical study of disk driven rotating MHD flow of a liquid metal in a cylindrical enclosure. *Acta Mechanica*, 135: 153-167. <https://doi.org/10.1007/BF01305749>

[12] Bessaih, R., Kadja, M., Eckert, K., Marty, P. (2003). Numerical and analytical study of rotating flow in an enclosed cylinder under an axial magnetic field. *Acta Mechanica*, 164: 175-188. <https://doi.org/10.1007/s00707-003-0021-x>

[13] Bessaih, R., Boukhari, A., Marty, P. (2009). Magneto-hydrodynamics stability of a rotating flow with heat transfer. *International Communications in Heat and Mass Transfer*, 36(9): 893-901. <https://doi.org/10.1016/j.icheatmasstransfer.2009.06.009>

[14] de Moro Martins, D.A., de Souza, F.J., de Vasconcelos Salvo, R. (2014). Formation of vortex breakdown in conical-cylindrical cavities. *International Journal of Heat and Fluid Flow*, 48: 52-68. <https://doi.org/10.1016/j.ijheatfluidflow.2014.05.001>

[15] Mahfoud, B., Bendjaghli, A., Laouari, A. (2018). MHD flow in a truncated conical enclosure. *Applied Journal of Environmental Engineering Science*, 4(2(sv)): 4-2. [https://doi.org/10.48422/IMIST.PRSM/aje-es-v4i2\(sv\).12909](https://doi.org/10.48422/IMIST.PRSM/aje-es-v4i2(sv).12909)

[16] Mahfoud, B. (2021). Magneto-hydrodynamic effect on vortex breakdown zones in coaxial cylinders. *European Journal of Mechanics-B/Fluids*, 89: 445-457. <https://doi.org/10.1016/j.euromechflu.2021.07.007>

NOMENCLATURE

U	dimensionless velocity vector
u	dimensionless radial velocity
v	dimensionless axial velocity
w	dimensionless azimuthal velocity
P	dimensionless pressure
R	container height base radius
R_t	top radius
A	aspect ratio
r, θ, z	dimensionless coordinates

Greek symbols

α	The angle of inclination ($^\circ$ degree)
Ω	angular velocity (rad/s)
ρ	fluid density (kg/m^3)
τ	dimensionless time
ν	kinematic viscosity, (m^2/s)

Subscripts

t	top
c	critical